IOP Publishing Semiconductor Science and Technology
Semicond. Sci. Technol. **29** (2014) 124003 (5pp) doi:10.1088/0268-1242/29/12/124003

Invited Article

Thermal conductivity of half-Heusler superlattices

Tino Jaeger[1], Paulina Hołuj[1,4], Christian Mix[1,4], Christoph Euler[1], Myriam Haydee Aguirre[2], Sascha Populoh[2], Anke Weidenkaff[2,3] and Gerhard Jakob[1]

[1] Institute of Physics, University of Mainz, Staudinger Weg 7, 55128 Mainz, Germany
[2] Solid State Chemistry and Catalysis Laboratory, Empa—Swiss Federal Laboratories for Materials Science and Technology, Ueberlandstrasse 129, 8600 Duebendorf, Switzerland
[3] Institute for Materials Science, University of Stuttgart, Heisenbergstr. 3, 70569 Stuttgart, Germany
[4] Graduate School Materials Science in Mainz, Staudinger Weg 9, 55128 Mainz, Germany

Received 8 April 2014, revised 10 July 2014
Accepted for publication 14 July 2014
Published 14 November 2014

Abstract

Thin films and superlattices (SLs) of TiNiSn and $Zr_{0.5}Hf_{0.5}NiSn$ layers have been grown by dc magnetron sputtering on MgO (100) substrates to reduce the thermal conductivity, aiming for improvement of the thermoelectric figure of merit *ZT*. The thermal conductivity of 1 $Wm^{-1}K^{-1}$ was measured by the differential 3ω method for an SL with a periodicity of 8.8 nm. In addition to x-ray diffraction analysis of the SL crystal structure, smooth interfaces were confirmed by scanning/transmission electron microscopy.

Keywords: thermoelectric, half-Heusler, superlattice, reduced thermal conductivity, 3 omega method, TiNiSn, Zr0.5Hf0.5NiSn

(Some figures may appear in colour only in the online journal)

Enhanced CO_2 emission and dwindling resources have moved thermoelectric (TE) materials into focus. Apart from energy recovery, heat management can be performed by TE devices. Independent of transforming heat into electrical energy or vice versa, the efficiency for TE materials depends on the figure of merit: $ZT = S^2\sigma\kappa^{-1}T$, relating temperature T, Seebeck coefficient S, electrical conductivity σ and thermal conductivity κ. Materials for TE devices should have $ZT > 1$, while the Carnot efficiency can be only reached in the limit of $ZT = \infty$.

Using nanostructured materials, *ZT*s have been enhanced by increased power factors $S^2\sigma$ or depressed thermal conductivities κ [1–4]. The thermal conductivity can be separated into contributions arising from electrons κ_{el} and phonons κ_{ph}. The electronic contribution is coupled to the electrical conductivity and therefore it is most important to minimize the phononic contribution by increased phonon scattering. Additional phonon scattering is obtained perpendicular to interfaces in superlattice (SL) structures [5–7]. Thus, Venkatasubramanian *et al* have achieved a *ZT* value of 2.4 after optimizing Bi_2Te_3/Sb_2Te_3 SLs [8]. Simultaneously, a depressed thermal conductivity and a less affected electron mobility have been found for a defined SL periodicity.

Here, artificial SLs containing well-defined half-Heusler (HH) compounds TiNiSn and $Zr_{0.5}Hf_{0.5}NiSn$ have been prepared in order to reduce the thermal conductivity [9–12]. Therefore, the variation of isoelectronic elements Ti, Zr and Hf was used to create mass fluctuations perpendicular to the film surface. The reduction of κ_{ph} due to enhanced mass fluctuations in homogeneous HH bulk samples (e.g. $Ti_x(Zr_{0.5}Hf_{0.5})_{1-x}NiSn$) has been already observed [13]. In addition, phase separation has been assigned to be responsible for depressed thermal conductivities in similar compounds [14, 15]. The fabrication of HH SLs enables the generation of artificial interfaces with desired distances for obtaining maximum phonon scattering.

Using dc magnetron sputtering, TiNiSn and $Zr_{0.5}Hf_{0.5}NiSn$ thin films and SLs of combined composition were fabricated on MgO (100) substrates. While TiNiSn and $Zr_{0.5}Hf_{0.5}NiSn$ sputter cathodes with a target diameter of 5 cm were continuously

operated for SLs fabrication, the MgO substrates were successively moved from one sputter cathode to the other. The substrate temperature was kept at about 450 °C, and Ar ambient pressures of 4.0 Pa were applied. TiNiSn and $Zr_{0.5}Hf_{0.5}NiSn$ sputter cathodes were operated with sputter powers of 26 W and 23 W, respectively. With a substrate-to-target distance of about 4 cm, growth rates of 1 nms^{-1} were achieved. The thicknesses of individual layers forming the SL periodicity were set by the time the substrates were in front of each cathode. This time was varied between 3 s and 30 s and was identical for both layers forming one SL.

At room temperature (RT), the differential 3ω method was utilized to determine the cross-plane thermal conductivity of thin films. Therefore, identical samples that only differed in HH film or SL thickness were generated [16, 17]. Thicker and thinner layers with thicknesses of about 700 nm and 100 nm were grown, resulting in a thickness difference of approximately 600 nm. Each sample, initially isolated with 200 nm of alumina, was capped by 50 nm of Au. Afterwards, 3ω heater structures were fabricated by optical lithography and wet-chemical etching. Heater stripes with lengths of 2 mm and widths of 20 μm were thereby generated, treating the Au layer. Beside the contact pads at both ends of the heater stripes, appropriate with a four-point-method, two contact pads were also connected in-between. The latter contact pads had a distance of 1 mm and were used to measure the voltage at the applied frequency U_ω and at the third harmonic $U_{3\omega}$. The applied current I_ω at the outer contact pads was set such that for each sample, a heating power I_ω U_ω of 18 mW dissipated between the inner contact pads. After subtracting U_ω , using a passive bridge circuit, $U_{3\omega}$ was measured by a SR850 DSP lock-in amplifier from Stanford Research Systems [18]. Temperature coefficients were accurately determined for each heater stripe by comparing $R = U_\omega I_\omega{}^{-1}$ with a Pt100 reference resistance at different ambient temperatures. Finally, applying a one-dimensional model, the difference in temperature oscillations caused by the difference in film thicknesses was used to calculate the thermal conductivity of the thin film [17, 19]. Each type of sample was grown twice and measured independently to obtain convincing thermal conductivities and reproducibility.

The van-der-Pauw method was applied to obtain in-plane conductivities for evaluating the electric contribution to the thermal conductivity κ_{el}. Afterwards, the Wiedemann–Franz law was used to estimate κ_{el}. For single films and SLs, the crystal quality was characterized by x-ray diffraction (XRD) $\theta/2\theta$ and ω scans. Additionally, electron diffraction (ED), high-resolution transmission electron microscopy (HRTEM) and scanning transmission electron microscopy (STEM) with a high angular annular dark field (HAADF) detector were performed to analyze the profiles of the films.

The epitaxial growth of single TiNiSn and $Zr_{0.5}Hf_{0.5}NiSn$ layers was successfully accomplished. While for $Zr_{0.5}Hf_{0.5}NiSn$, better crystal growth was obtained on a TiNiSn buffer layer, epitaxial TiNiSn layers were directly deposited on MgO (100). For both HH films, crystallite sizes of about 90 nm were measured by XRD. Due to the low lattice mismatch of 0% and 1.5% for TiNiSn and $Zr_{0.5}Hf_{0.5}NiSn$ on MgO (100), respectively, a favored in-plane growth direction has already been obtained [20]. Simultaneously, elemental compositions of deposited TiNiSn and $Zr_{0.5}Hf_{0.5}NiSn$ layers were affirmed by Rutherford backscattering and energy-dispersive x-ray spectroscopy.

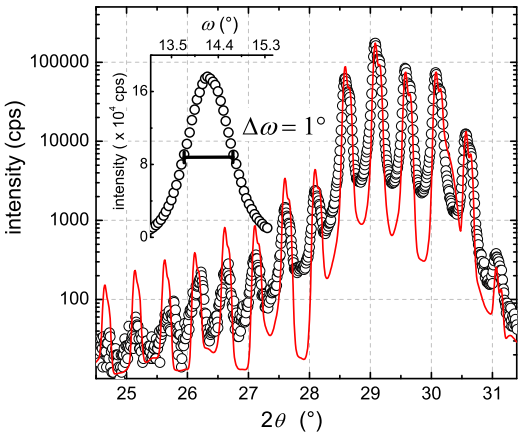

Figure 1. XRD $\theta/2\theta$ and ω (inset) scans of an SL with a periodicity of about 20 nm (a fitted periodicity equal to 18.4 nm—details are in the text).

In addition to ordered atomic planes in SLs, parallel to the surface a further periodicity arises due to alternating layers. In the case of an SL containing TiNiSn and $Zr_{0.5}Hf_{0.5}NiSn$ with similar lattice constants, in XRD $\theta/2\theta$ scans an SL creates satellite peaks close to the diffraction spots of the individual layers [21]. For a TiNiSn/$Zr_{0.5}Hf_{0.5}NiSn$ SL with a periodicity of about 20 nm and homogeneously contributed layers, the satellite peak structures at the (200) diffraction spots of individual layers are shown in figure 1. The shape of the satellite peaks is asymmetric due to Cu $K_{\alpha 1}$ and $K_{\alpha 2}$ radiation, indicating a structural coherence length that ranges over several SL periods. The red line in figure 1 shows the intensity calculated for a coherent scattering from a perfect $(TiNiSn_{9.3\ nm}/Zr_{0.5}Hf_{0.5}NiSn_{9.1\ nm})_{20}$ SL on a 30 nm TiNiSn buffer layer. The lattice constants of the materials were determined from the simulation to be 5.91 Å and 6.17 Å, respectively. It can be assumed that an in-plane lattice alignment of both cubic HH compounds at the interfaces causes this observed strain [20]. Thus, the in- and out-of-plane lattice constants for single TiNiSn layers are elongated and compressed, respectively. The alignment for $Zr_{0.5}Hf_{0.5}NiSn$ is assumed to be the opposite. Deviations for higher order satellite peaks indicate some thickness fluctuations and roughness in the SL. Taken from the most intense satellite peak, the full width at half maximum (FWHM) of the XRD ω scan (inset) of 1° indicates only a small tilt between different grains.

Additionally, another sample was investigated using ED. As is shown in figure 2(a), SL diffraction spots were also confirmed by ED [22]. The [110] zone axis shows SL spots (arrow marks) with a periodicity of 2.9–3 nm. Thus, an SL structure with interfaces now perpendicular to the surface can be visualized by an STEM–HAADF image (figure 2(b)) and an HRTEM image (figure 2(c)). According to the quadratic

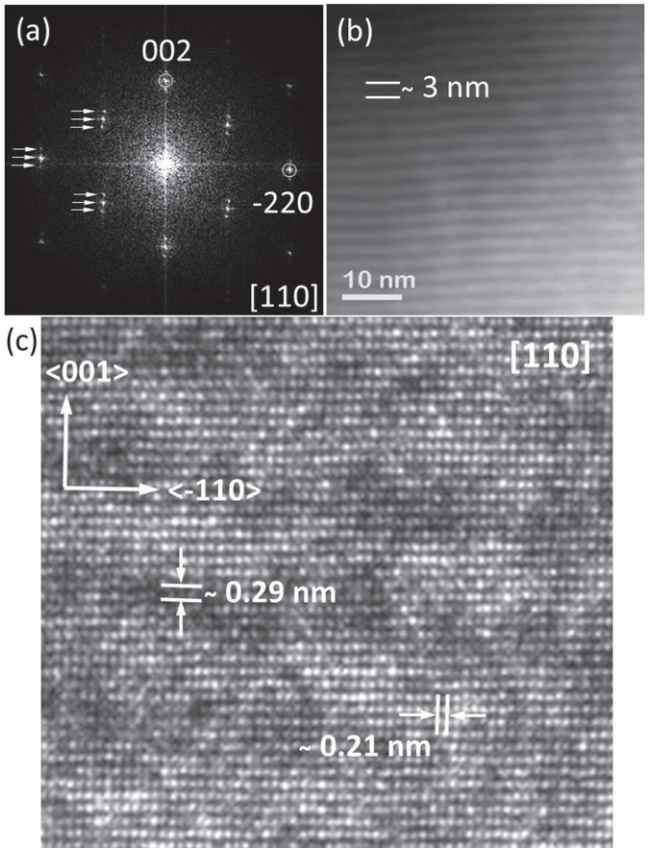

Figure 2. a) ED of [110] zone axis showing the extra SL diffraction spots; b) STEM–HAADF image of an SL with TiNiSn in dark contrast and $Zr_{0.5}Hf_{0.5}NiSn$ in white contrast; c) HRTEM showing the atomic arrangement in the [110] zone axis of an HH SL.

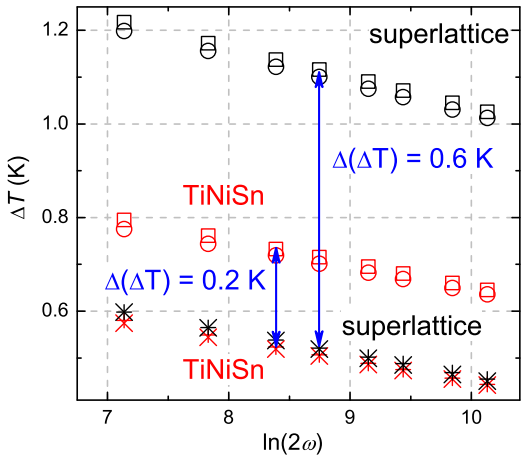

Figure 3. ΔT at varied frequencies $\ln(2\omega)$ for two sets of samples. The thermal conductivities of TiNiSn (red) and an SL with a periodicity of 8 nm (black) were obtained by the differences in ΔT between thicker samples (squares, circles) and reference/thinner samples (crosses, tilted crosses).

dependency of the atomic weight on the STEM–HAADF image intensity, dark- and light-grey layers can be attributed to TiNiSn and $Zr_{0.5}Hf_{0.5}NiSn$ (see figure 2(b)), respectively. A different contrast can be detected in HRTEM, but in this case it cannot be directly assigned to a specific composition, since bright field techniques are affected by more parameters such as diffraction and thickness contrast. Grains with a columnar structure were observed for ongoing film growth. Following the grain boundary, well-ordered SL growth was observed.

In order to obtain the thermal conductivity of single HH films and SLs, $U_{3\omega} = f(\ln(2\omega))$ was measured for each sample. Using ΔT, which can be derived from $U_{3\omega}$, the results from two sets of samples with a higher and a lower thermal conductivity are illustrated in figure 3. Here, the differences in ΔT at a given frequency were determined by the thermal resistances between heater stripes and substrates. As well as the thermal conductivity of a film, its thickness also influences ΔT. While the thickness of the reference samples (crosses, tilted crosses) was not sufficient to create a significant difference in thermal resistance between the heater and the substrate, ΔT varied clearly for films with thicknesses of about 700 nm (circles, squares). Due to varied thermal conductivities, a significant difference in ΔT was obtained for TiNiSn (red) and an SL with a periodicity of about 8 nm (black). Here, the lower thermal conductivity of the SL created a higher ΔT at an identical applied power. Finally, the thermal conductivity of the film was determined by $\Delta(\Delta T)$. Average values and maximum deviations of the thermal conductivities were determined by the ΔT taken from two thicker and two thinner samples. Because in the range of the applied frequency, the thermal conductivity of the MgO substrate accounts for the slope of $\Delta T = f(\ln(2\omega))$, $\Delta(\Delta T)$ does not change with frequency [16].

At RT, a thermal conductivity of 2.8 ± 0.1 $Wm^{-1}K^{-1}$ was obtained for the thin film TiNiSn. A lowered thermal conductivity compared to TiNiSn bulk samples was measured due to the reduced grain sizes [23]. A thermal conductivity of 1.10 ± 0.05 $Wm^{-1}K^{-1}$ was calculated for $Zr_{0.5}Hf_{0.5}NiSn$. Compared to TiNiSn, enhanced mass fluctuation as well as increased atomic weights, induced by Zr and Hf, account for the reduction of the thermal conductivity [24–26]. Among others, the structural quality of the thin films is demonstrated by the FWHM taken from the XRD rocking curves. For TiNiSn, 0.77° was obtained for the FWHM of the rocking curve taken at the (200) diffraction peak. An increased FWHM of 1.8° was measured for $Zr_{0.5}Hf_{0.5}NiSn$ and indicates a depressed crystal quality. The depressed crystal quality that is also expressed by a reduced diffraction peak intensity (not shown) contributes to the decreased thermal conductivity of the $Zr_{0.5}Hf_{0.5}NiSn$ layer. Therefore, enhanced atomic weight, increased mass fluctuation and depressed crystal quality cause the extraordinary low thermal conductivity of $Zr_{0.5}Hf_{0.5}NiSn$. In addition to the low thermal conductivity of $Zr_{0.5}Hf_{0.5}NiSn$, the much higher thermal conductivity of TiNiSn complicates the investigation of interface effects. In the case of a homogeneously contributed bilayer, composed by TiNiSn (κ = 2.8 $Wm^{-1}K^{-1}$) and $Zr_{0.5}Hf_{0.5}NiSn$ (κ = 1.1 $Wm^{-1}K^{-1}$), a mean thermal conductivity of 1.56 $Wm^{-1}K^{-1}$ can be calculated if interface effects are neglected and the thermal conductivity of the HH layers remains unchanged [7].

For films and SLs with varied periodicities, the thermal conductivities and FWHMs of rocking curves of the most

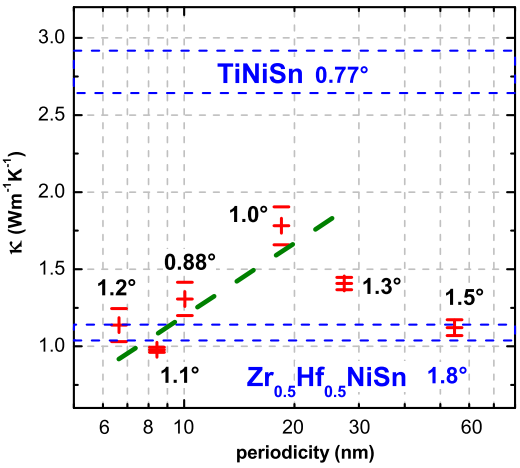

Figure 4. Cross-plane thermal conductivity measured for single HH films (blue) and TiNiSn/$Zr_{0.5}Hf_{0.5}$NiSn SLs with different modulation lengths.

intense XRD film peaks are given in figure 4. With a periodicity of 18.4 nm, the SL with the highest thermal conductivity of 1.78 ± 0.12 $Wm^{-1}K^{-1}$ was measured. Compared to the supposed bilayer above, an increased thermal conductivity was found. An argumentation leading to a false negative interface conductance was avoided by the dependency of the thermal conductivity on the structural quality of single layers. Here, indicating a well-ordered SL, the FWHM of the rocking curve taken at the most intense satellite peak was measured to be 1.0°. Since the thermal conductivity is also influenced by lattice imperfections, the enhanced thermal conductivity in the SL with a periodicity of 18.4 nm was most likely obtained by the higher crystal quality of the $Zr_{0.5}Hf_{0.5}$NiSn layers in the SL compared to single $Zr_{0.5}Hf_{0.5}$NiSn films. Depressed thermal conductivity was found along lower and higher SL periodicities. The thermal conductivity of the SLs was not dominantly influenced by interface scattering at higher SL periodicities with interface densities of 36.6 μm^{-1} and 18.3 μm^{-1}. Similar to single $Zr_{0.5}Hf_{0.5}$NiSn films, broadened XRD rocking curves were obtained for the SLs with large periodicities. This indicates that inferior film growth of single $Zr_{0.5}Hf_{0.5}$NiSn layers is transferred to TiNiSn layers and reduces the structural quality of these SLs. Therefore, it can be concluded that there is a relation between the tilt of several crystallites and the thermal conductivity. Notably, a similar trend and argumentation can be found for Si/Ge SLs [5]. Due a transition of the Ge growth mode on Si, from planar films to Ge nanodots, comparable crystal structures for Si/Ge SLs can be obtained only for limited Ge layer thickness [28, 29]. Here, increasing the $Zr_{0.5}Hf_{0.5}$NiSn layer thickness reduces the epitaxial quality, which cannot be remedied by the intermediate TiNiSn layers.

At lower SL periodicities, the influence of interface scattering becomes apparent. For interface densities higher than 54.3 μm^{-1} (which corresponds to an SL periodicity of 18.4 nm), a trend (green dashed line) to lower thermal conductivities can be seen. At interface densities of 99.5 μm^{-1} and 118.6 μm^{-1}, thermal conductivities of 1.31 ± 0.11 $Wm^{-1}K^{-1}$ and 0.98 ± 0.02 $Wm^{-1}K^{-1}$, respectively, were determined. In contrast to the SLs with larger SL periodicities, here SLs with a better or a similar epitaxial quality exhibited a thermal conductivity that is lower than previously calculated for the theoretically supposed bilayer. Furthermore, a slightly enhanced thermal conductivity was found for an SL with a higher interface density. The SL with a periodicity of 6.6 nm and thus the highest interface density of 151.5 μm^{-1} exhibited a thermal conductivity of 1.14 ± 0.15 $Wm^{-1}K^{-1}$. For similar periodicities, the lowest thermal conductivities were also observed for ZrN/ScN and Bi_2Te_3/Sb_2Te_3 SLs [7, 27]. The influence of the structural film quality is decisive for the interface scattering effect on the thermal conductivity.

σ was measured in-plane to assess the contribution of κ_{el} to the total thermal conductivity, which was determined by the differential 3ω method. The electrical conductivity was measured to be 2.5 x 10^5 Sm^{-1} for SLs and single films at RT. About 0.2 $Wm^{-1}K^{-1}$ of the thermal conductivity could be addressed to κ_{el}, since only negligible variations of σ were measured parallel to the film surface for all samples. Enhanced electron scattering at the interfaces is not expected in the selected HH material system. Perpendicular to the interfaces of the SLs, σ might be reduced. In this particular case, κ_{el} of SLs would be decreased and dependent on the SL periodicity. Experiments for measuring σ cross-plane are in progress to study the influence of the interfaces on the κ_{el}.

In conclusion, SL consisting of TiNiSn and $Zr_{0.5}Hf_{0.5}$NiSn were grown by dc magnetron sputter deposition with sharp interfaces and a structural coherence ranging over several SL periods. Compared to similar HH bulk samples, reduced thermal conductivities were found for all thin films. Using HH SLs, a lowest thermal conductivity of about 1 $Wm^{-1}K^{-1}$ was measured. Importantly, this value, obtained from an SL with a periodicity of 8.4 nm, is much smaller than the mean value of individually measured TiNiSn and $Zr_{0.5}Hf_{0.5}$NiSn films. However, additional optimization steps of HH thin films and SLs are necessary to observe a more systematic reduction of the thermal conductivity. Further studies on TE properties will reveal if the reduced thermal conductivities can contribute to increased *ZT* values in nanostructured films.

Acknowledgements

We gratefully acknowledge financial support by DFG Ja821/4–2 within priority program SPP 1386 and the Graduate School of Excellence *Material Science in Mainz* (DFG/GSC 266).

References

[1] Hicks L D and Dresselhaus M S 1993 *Phys. Rev.* B **47** 12727
[2] Snyder G J and Toberer E S 2008 *Nat. Mater.* **7** 105
[3] Shakouri A 2011 *Annu. Rev. Mater. Res.* **41** 399

[4] Xie W, Weidenkaff A, Tang X, Zhang Q, Poon J and Tritt T M 2012 *Nanomaterials* **2** 379
[5] Lee S-M, Cahill D G and Venkatasubramanian R 1997 *Appl. Phys. Lett.* **70** 2957
[6] Huxtable S T *et al* 2002 *Appl. Phys. Lett.* **80** 1737
[7] Rawat V, Koh Y K, Cahill D G and Sands T D 2009 *J. Appl. Phys.* **105** 024909
[8] Venkatasubramanian R, Siivola E, Colpitts T and O'Quinn B 2001 *Nature* **413** 597
[9] Jeitschko W 1970 *Metall. Mater. Trans.* B **1** 3159
[10] Graf T, Felser C and Parkin S S P 2011 *Prog. Solid State Chem.* **39** 1
[11] Kimura Y, Ueno H and Mishima Y 2009 *J. Electron. Mater.* **38** 934
[12] Muta H, Kanemitsu T, Kurosaki K and Yamanaka S 2009 *J. Alloys Compd.* **469** 50
[13] Sakurada S and Shutoh N 2005 *Appl. Phys. Lett.* **86** 082105
[14] Populoh S, Aguirre M H, Brunko O C, Galazka K, Lu Y and Weidenkaff A 2012 *Scripta Mater.* **66** 1073
[15] Schwall M and Balke B 2013 *Phys. Chem. Chem. Phys.* **15** 1868
[16] Cahill D 1990 *Rev. Sci. Instrum.* **61** 802
Cahill D 2002 *Rev. Sci. Instrum.* **73** 3701
[17] Lee S-M and Cahill D G 1997 *J. Appl. Phys.* **81** 2590
[18] Raudzis C E, Schatz F and Wharam D 2003 *J. Appl. Phys.* **93** 6050
[19] Borca-Tasciuc T, Kumar A R and Chen G 2001 *Rev. Sci. Instrum.* **72** 2139
[20] Jaeger T, Mix C, Schwall M, Kozina X, Barth J, Balke B, Finsterbusch M, Idzerda Y U, Felser C and Jakob G 2011 *Thin Solid Films* **520** 1010
[21] Fullerton E R, Schuller I K, Vanderstraeten H and Bruynseraede Y 1992 *Phys. Rev.* B **45** 9292
[22] Jia C L, Soltner H, Jakob G, Hahn T, Adrian H and Urban K 1993 *Physica* C **210** 1
[23] Bhattacharya S, Skove M J, Russell M, Tritt T M, Xia Y, Ponnambalam V, Poon S J and Thadhani N 2008 *Phys. Rev.* B **77** 184203
[24] Hohl H, Ramirez A P, Goldmann C, Ernst G, Woelfing B and Bucher E 1999 *J. Phys.: Condens. Matter* **11** 1697
[25] Sharp J W, Poon S J and Goldsmid H J 2001 *Phys. Status Solidi a* **187** 507
[26] Abeles B 1963 *Phys. Rev.* **131** 1906
[27] Venkatasubramanian R 2000 *Phys. Rev.* B **61** 3091
[28] Chen P, Katcho N A, Feser J P, Li W, Glaser M, Schmidt O G, Cahill D G, Mingo N and Rastelli A 2013 *Phys. Rev. Lett.* **111** 115901
[29] Mo Y-W, Savage D E, Swartzentruber B S and Lagally M G 1990 *Phys. Rev. Lett.* **65** 1020